Influence of the Anion on Lone Pair Formation in Sn(II) Monochalcogenides: A DFT Study

Aron Walsh and Graeme W. Watson*

Department of Chemistry, University of Dublin, Trinity College, Dublin 2, Ireland

Received: April 8, 2005; In Final Form: August 8, 2005

The electronic structure of SnO, SnS, SnSe, and SnTe in the rocksalt, litharge, and herzenbergite structures has been calculated using density functional theory. Comparison of the distorted and undistorted structures allows for an explanation of the unusual experimentally observed structural transitions seen along the Sn(II) monochalcogenides. Analysis of the electronic structure shows a strong anion dependence of the Sn(II) lone pair, with the Sn(5s) and Sn(5p) states too far apart to couple directly. However, the interaction of Sn(5s) with anion states of appropriate energy produce a filled antibonding Sn(5s)−anion p combination which allows coupling of Sn(5s) and Sn(5p) to occur, resulting in a sterically active asymmetric density on Sn. While the interaction between Sn(5s) and O(2p) is strong, interactions of Sn with S, Se, and Te become gradually weaker, resulting in less high energy 5s states and hence weaker lone pairs. The stability of the distorted structures relative to the symmetric structures of higher coordination is thereby reduced, which induces the change from highly distorted litharge SnO to highly symmetric rocksalt SnTe seen along the series.

1. Introduction

Sn(II) compounds possess a wide range of potential applications including nanowires,[1] superconducting crystals,[2] rechargeable batteries,[3] and solar cells.[4] The development of new Sn materials requires a better understanding of the underlying electronic structure, and crucial to this is knowledge of the Sn(II) lone pair and its effect on crystal structure and phase stability. With a filled 5s subshell and an electronic configuration of $4d^{10}5s^25p^0$, the classical view of Sn(II) is that after hybridization of the s and p orbitals the Sn $5s^2$ electrons occupy an inert orbital[5] projected out one side of the Sn. This pair of electrons is thus considered a chemically inactive lone pair[6,7] which is sterically active in distorting the crystal structure. However, the lone pair is not always present, and distortion of the crystal structure does not always occur, with a number of Sn(II) compounds adopting symmetric crystal structures. This implies that the formation and stability of the lone pair is more complicated than classical hybridization alone would suggest.

A clear example of this are the Sn(II) monochalcogenides, SnX (X = O, S, Se, and Te), which exist in very different crystalline environments despite having similar electronic configurations. SnO adopts a layered tetragonal[8] structure (litharge), space group *P*4/*nmm*, with each Sn atom positioned at the apex of a square pyramid formed by four oxygen atoms (Figure 1a). This structure can be seen as a distortion of the eight-coordinate, cubic CsCl structure through elongation of the *c* axis. In contrast, the perfectly symmetric rocksalt structure, space group *Fm*3*m*, is adopted by SnTe as its thermodynamically stable phase (Figure 1b). SnS and SnSe both assume a layered orthorhombic structure (herzenbergite), space group *Pnma* (Figure 1c). This structure consists of strongly bound double layers stacked along the *a* axis and can be seen as a severe distortion of the rocksalt phase, producing three-coordinate oxygen coordination around each Sn atom. SnSe has also been described as being metastable in the rocksalt structure and as being a borderline case between the cubic and orthorhombic phases.[9] Indeed, the close relationship between rocksalt and the distorted orthorhombic phase has been well explored with SnS and SnSe seen to adopt the NaCl structure when grown on rocksalt substrates,[10] indicating a small energy difference between the phases.

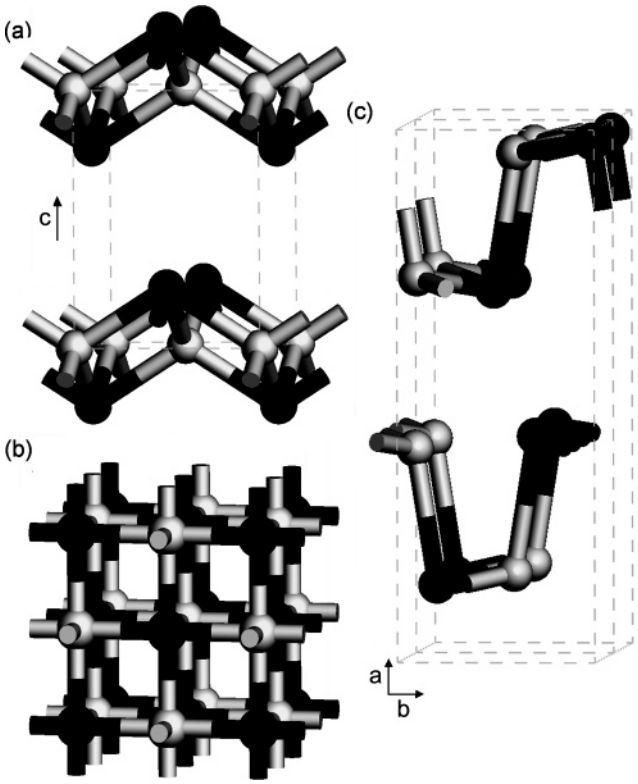

Figure 1. Crystal structures of (a) litharge SnO, (b) rocksalt SnTe, and (c) herzenbergite SnS. The Sn atoms are colored dark with the anions light.

Density functional theory (DFT) and tight binding calculations have been performed on this series of compounds by Lefebvre

* Corresponding author: Tel +353 1 6081357; e-mail watsong@tcd.ie.

10.1021/jp051822r CCC: $30.25
Published on Web 09/17/2005

et al.,[11] although their emphasis was not on the formation of the lone pair. The electronic structures were only calculated in their observed crystalline structure, and as such, the behavior of the Sn(II) asymmetry through the series could not be addressed. Previous local density approximation DFT calculations on SnO[12] in the litharge and CsCl structures first indicated that O(2p) states are involved in the states responsible for the Sn(II) lone pair. Bernasconi et al.[13] examined the polarizibility of a SnO molecule in the gas phase at the GGA level. While hybridization of O(2p) with unfilled Sn(5p) states is predicted, any analysis of the lone pair states is restricted through the limited approach taken, examining only the partitioned charge density resulting from Wannier decomposition.

Electronic structure calculations have also been performed on PbO[14] which suggest that the formation of the Pb(II) lone pair and the stabilization of the distorted litharge structure are not purely the result of the Pb $6s^2$ electrons. In addition, a recent study of both PbO and PbS[15] has concluded that the anion does play a key role in the formation of the Pb(II) lone pair. DFT calculations have performed on both litharge PbO and SnO by Raulot et al.[16] although their focus was on electron densities and ELF's of lone pairs rather than on their electronic origin. Waghmare et al.[17] used DFT to study the rocksalt chalcogenides of Ge, Pb, and Sn, and although they observed changes in the calculated electronic structure for different anions, they could not comment on lone pair formation as their studies main focus was the symmetric rocksalt structure. In a more recent study[18] we have performed generalized gradient approximation (GGA) DFT calculations on SnO in the rocksalt, litharge, and herzenbergite crystal structures which showed that the distortion of the Sn(II) electron density in SnO arises directly from a interaction between Sn(5p) and the filled antibonding combination arising from the interaction of Sn(5s) and O(2p).

The aim of this study is to examine the effect of the anion on lone pair formation and phase stability of the SnX series by calculating the electronic structure of SnO, SnS, SnSe, and SnTe in the rocksalt, litharge, and herzenbergite crystal structures, the thermodynamically stable phases of the Sn(II) monochalcogenides. Electronic structure analysis of each phase should give a better understanding to the origin of electron distribution in Sn(II) as well as explaining the unusual crystallographic behavior exhibited by the Sn(II) monochalcogenides.

2. Computational Methods

In this study all electronic structure calculations are performed using DFT as embodied in the Vienna Ab-initio Simulation Package[19−21] (VASP). The exchange and correlation energy are evaluated within the GGA using the parametrization of Perdew et al.[22] with the crystal wave functions expanded in terms of a plane wave basis set using periodic boundary conditions. The Kohn−Sham equations[23] were solved self-consistently using a blocked Davidson iterative matrix diagonalization scheme. The forces on the atoms were calculated using the Hellmann−Feynman theorem, which were used to perform a quasi-Newton relaxation until they had converged to less than 0.005 eV/Å, and the pressure on the cell had equalized. The projector augmented wave method[24] (PAW) was used to accurately represent valence−core (Sn: [Kr], O: [He], S: [Ne], Se: [Ar], Te: [Kr]) interactions.

The plane wave cutoff energy and *k*-point density, the latter which was obtained using the Monkhorst−Pack[25] method, were both checked for convergence for each system, to within 0.01 eV/Sn. A plane wave cutoff of 500 eV was used for SnO with a 400 eV cutoff for SnS, SnSe, and SnTe. A *k*-point grid density of $8 \times 8 \times 8$ was used for the reduced two atom rocksalt unit cell with densities of $6 \times 6 \times 4$ and $2 \times 6 \times 6$ used for the litharge and herzenbergite phases, respectively.

TABLE 1: Calculated Structural Data and Relative Binding Energies for Rocksalt, Litharge, and Herzenbergite Structured SnO, SnS, SnSe, and SnTe, with % Error with Respect to Experiment[7,19] Where Available

	rocksalt	litharge	herzenbergite
SnO			
rel BE (eV/Sn)	+0.89	0.00	+0.19
a (Å)	5.116	3.867 (+1.7%)	11.784
b (Å)		3.867 (+1.7%)	3.403
c (Å)		5.036 (+4.1%)	3.950
band gap (eV)	0.187	1.148	0.520
SnS			
rel BE (eV/Sn)	+0.18	+0.26	0.00
a (Å)	5.848	4.882	11.439 (+2.1%)
b (Å)		4.882	4.033 (+1.2%)
c (Å)		4.610	4.396 (+1.4%)
band gap (eV)		0.623	1.352
SnSe			
rel BE (eV/Sn)	+0.01	+0.30	0.00
a (Å)	6.062	5.171	11.741 (+2.1%)
b (Å)		5.171	4.207 (+1.3%)
c (Å)		4.445	4.571 (+2.8%)
band gap (eV)		0.509	1.108
SnTe			
rel BE (eV/Sn)	0.00	+0.39	+0.10
a (Å)	6.312 (+1.5%)	5.542	12.378
b (Å)		5.542	4.531
c (Å)		4.116	4.757
band gap (eV)			0.801

3. Results

a. Optimization of the Lattice Vectors. A series of fixed volume optimizations were carried out for SnO, SnS, SnSe, and SnTe in each of the three phases (rocksalt, litharge, herzenbergite). Within these calculations the atom positions and the lengths and the angles of the lattice vectors are allowed to vary within the constraint of constant volume, giving rise to a set of energy volume data. The equilibrium volume was obtained by fitting the resulting curve to the Murnaghan equation of state.[26] By performing an additional constant volume calculation at the equilibrium cell volume, the final structure is obtained. This approach helps avoid the problem of the Pulay stress and changes in basis set that occur in plane wave calculations on volume changes.[27]

The calculated relative binding energies and lattice vectors for each structure are listed in Table 1. The lattice vectors for the thermodynamically stable structures show good agreement with experimental values.[7,28] The *c* lattice vector which represents the interlayer distance in litharge SnO is overestimated to a greater extent (4.1%) due to the inability of DFT to accurately describe the weak nature of the forces in this direction. However, the stable phase is correctly predicted, and the Sn−O interatomic distances are calculated at 2.26 Å, within 1.7% of experiment, indicating a good representation of the strong bonding and phase stability of SnO.

While the binding energies predict litharge as the lowest energy SnO structure as would be expected for the thermodynamically stable phase, it is calculated as being the least stable structure for SnS, SnSe, and SnTe. The thermodynamically stable phase of both SnS and SnSe is the distorted herzenbergite structure, and while this is reflected as a stable structure in our binding energies, the calculations predict the rocksalt structure to be only 0.18 eV/Sn less stable than herzenbergite for SnS and 0.01 eV/Sn less stable than herzenbergite for SnSe. The

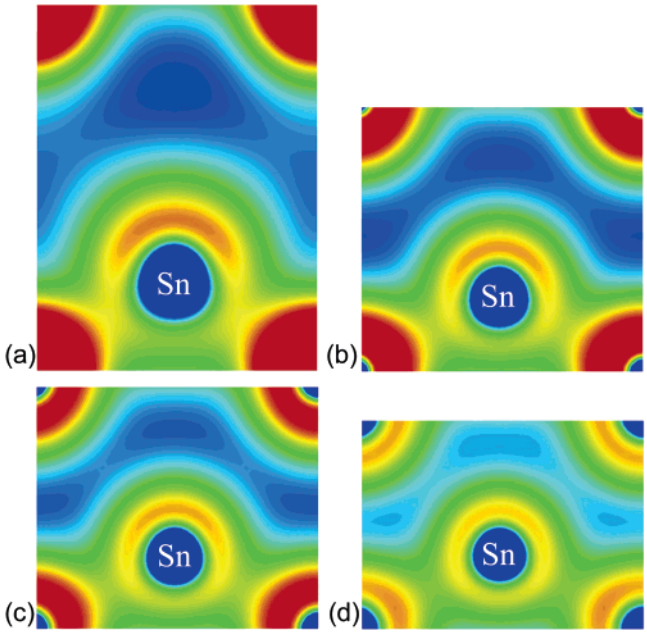

Figure 2. Electron density contour maps for (a) SnO, (b) SnS, (c) SnSe, and (d) SnTe in the litharge structure, taken through the (100) plane containing a Sn atom toward the center with four anions positioned at each of the corners. Contour levels shown are between 0 (blue) and 0.5 e/Å^3 (red).

small energy difference between the rocksalt structure and the distorted orthorhombic phase for is as expected from previous studies.[9,10] Rocksalt is correctly predicted as the stable phase of SnTe with both distorted structures higher in energy.

The lattice vector of the rocksalt structure increases through the series as expected with anions of increasing size. The litharge structure also undergoes similar expected increases for its *a* and *b* vectors, while the *c* vector undergoes a reduction, reducing almost linearly from 5.04 Å in SnO to 4.12 Å in SnTe, significantly below that expected from the SnO *a*:*c* ratio (7.22 Å). This corresponds to a reduction in the interlayer distance which can be seen as an attempt to return to the undistorted, eight-coordinate CsCl structure. For SnTe this is not unexpected as experimentally it does not show a stereochemically active lone pair, and no distorted structures have been observed. This would suggest that significant differences in the electronic structure along the series must exist, resulting in these observed structural changes of the optimized litharge structure. Optimization of SnO in the herzenbergite structure resulted in an expansion of the *a* vector by 3% relative to the experimental SnS structure. This is somewhat unexpected considering that oxygen is the smaller anion, but again could be related to lone pair activity. The *a* vector then increases with anion size from SnS to SnTe.

b. Electron Densities. The valence electron densities arising from states between −10 eV and the highest occupied state were calculated for each material and are shown for litharge through the (100) plane (Figure 2) and for herzenbergite through the (110) plane (Figure 3). The X(s) and Sn(4d) states both occur at lower energies; however, they make no significant contribution to chemical bonding and have been excluded for clarity of the remaining states. The electron density maps for rocksalt show symmetric electron distribution around both Sn and the anion for all compounds (not shown), as expected for symmetric Sn coordination. The densities for litharge SnO show a uniform electron distribution around the oxygen atoms with Sn forming an enhanced electron density (lone pair) directed in the *c* direction, pointing away from the Sn−O layers. A progressively weaker distortion can be seen to form from SnO to SnTe, with the Sn electron density becoming more symmetric through the series. By SnTe the Sn electron distribution is almost spherical. As the lone pair produced by Sn(II) is considered responsible for directing the layered structure, the reduction in the *c* vector of the litharge structure along the series can be understood from the decrease in the strength of the Sn lone pair observed in the electron density maps. The electron density maps for herzenbergite display a similar trend. The Sn atoms in herzenbergite SnO feature a strong lone pair directed away from the Sn atom which is subsequently reduced from SnS to SnTe.

c. Partial Electron Density of States. To examine in detail the effect of the anion on the electronic density of states, the partial (ion and *l* and *m* quantum number decomposed) electronic density of states (PEDOS) has been calculated and is displayed for rocksalt (Figure 4), litharge (Figure 5), and herzenbergite (Figure 6) from −10 to +5 eV, relative to the highest occupied state. These were calculated by projecting the wave functions onto spherical harmonics centered on each atom with a radius of 1.55 Å for Sn and 1.6, 1.75, 1.9, and 2.1 Å for the O, S, Se, and Te atoms, respectively, which give rise to reasonable space filling and the correct total number of electrons. The results are qualitatively insensitive to changes in these radii.

The PEDOS possess a number of common features, allowing for the area below the Fermi level to be divided into three main regions. The lowest energy region (region I) running from approximately −9 to −6 eV consists of both Sn(5s) and X(p) states with the second region (region II), mainly occupied by X(p) states, running from around −6 to −3 eV. The third region (region III) appears from approximately −3 eV to the Fermi level and contains mainly a mixture of Sn(5s) and X(p) states.

The rocksalt structure features the most defined peaks with the PEDOS of all structures reflecting its high symmetry (Figure 4). For rocksalt SnO region I consists of almost equal amounts of Sn(5s) and O(2p) character with a clear gap between region I and the beginning of the region II states at −6 eV. Region II contains a large well-defined O(2p) peak between −6 and −3 eV with a small amount of Sn(5p) character also present. Region III consists of ∼70% O(2p), 25% Sn(5s), and 5% Sn(5p) character with a gap of 0.19 eV between the valence and conduction bands. For SnS, SnSe, and SnTe a number of changes occur. First, there is a significant reduction in the in the X(p) character present in region I, from 50% in SnO to approximately 35%, 30%, and 25% in SnS, SnSe, and SnTe, respectively. These changes are also accompanied by a similar reduction in the high-energy region III Sn(5s) states from 25% in SnO to 10% in SnTe. We have calculated the splitting between the center of the region I peak, where the majority of Sn(5s) states are located, and the top of region II, which lies between the region II and region III O(2p) states. This yields a qualitative value of the energy difference between Sn(5s) and X(p) states. For rocksalt this splitting increases from 3.5 eV in SnO to 5.25, 5.5, and 5.75 eV in SnS, SnSe, and SnTe, respectively. There is clear shift of anion p states to higher energy through the series, relative to Sn(5s), with the region II states gradually merging with region III.

The peaks in the PEDOS of the litharge structure are less uniform (Figure 5). While the compositions of each region are comparable to those of rocksalt, for litharge SnO there is the additional presence of Sn($5p_z$) overlapping with the O(2p) and Sn(5s) states in region III just below the Fermi level. There is also substantial overlap between regions I and II with the central O(2p) peak spread over a wide range, from −6 eV to almost −1.5 eV. Region III is composed of approximately 50% O(2p),

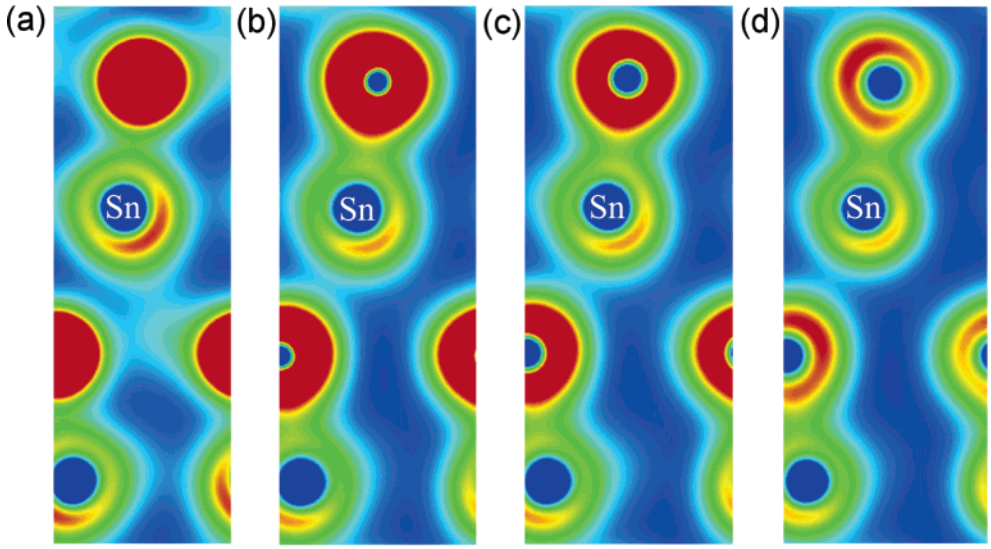

Figure 3. Electron density contour maps for (a) SnO, (b) SnS, (c) SnSe, and (d) SnTe in the herzenbergite structure, taken through the (010) plane containing two Sn anion pairs with the Sn atom positioned at the lower end of each pair. Contour levels shown are between 0 (blue) and 0.4 e/Å^3 (red).

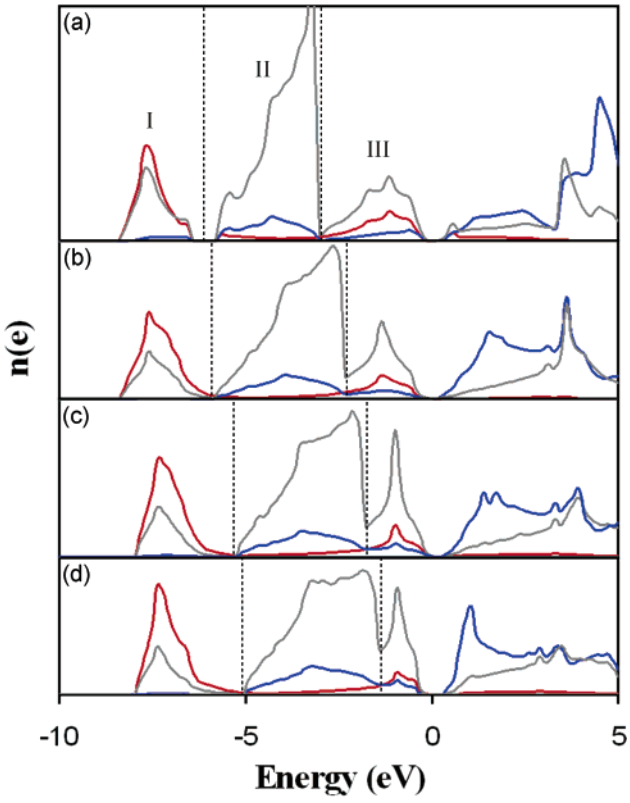

Figure 4. Partial electron density of states for (a) SnO, (b) SnS, (c) SnSe, and (d) SnTe in the rocksalt structure, relative to the highest occupied state. The red lines correspond to Sn(5s) states, blue to Sn(5p), and gray to X(p) states. The regions of the valence band are distinguished by the dashed lines.

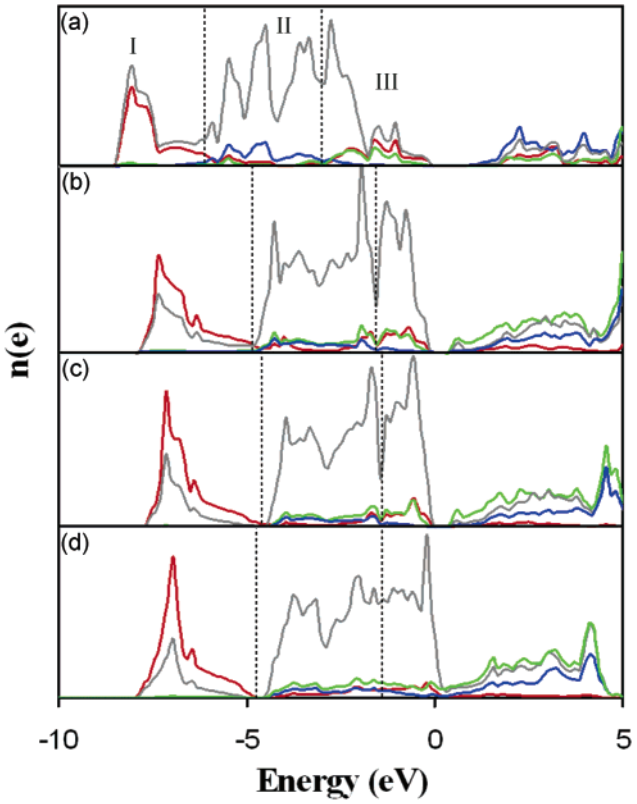

Figure 5. Partial electron density of states for (a) SnO, (b) SnS, (c) SnSe, and (d) SnTe in the litharge structure, relative to the highest occupied state. The red lines correspond to Sn(5s) states, blue to Sn($5p_x + p_y$), green to Sn($5p_z$), and gray to X(p) states. The regions of the valence band are distinguished by the dashed lines.

30% Sn(5s), and 20% Sn($5p_z$) character in litharge SnO. The states at the top of the valence band are shifted away from the Fermi level with a band gap of almost 1.2 eV present. This is significantly underestimated taking into account the photoemission determined gap[29] of around 2.5 eV, a well-documented failure of DFT. Also of interest is the appearance of an unoccupied Sn(5s) peak above the Fermi level at +3 eV, which was not present in rocksalt SnO. The reduction of anion p states in region I and of Sn(5s) states in region III observed for rocksalt is again seen to occur through the series, with an almost negligible amount of Sn(5s) character present in region III of SnTe. A number of additional changes also occur. For litharge SnS there is no significant shift of the near Fermi level states away from the Fermi level, and the band gap is reduced to 0.62 eV (Figure 5b). This trend continues with a band gap of 0.51 eV for litharge SnSe and litharge structured SnTe showing no gap at the Fermi level. Similar to rocksalt, the splitting between the center of the region I peak and the top of region II increases from 5.0 eV in SnO to 5.2, 5.3, and 6.5 eV in SnS, SnSe, and SnTe, respectively. The unoccupied Sn(5s) states are also

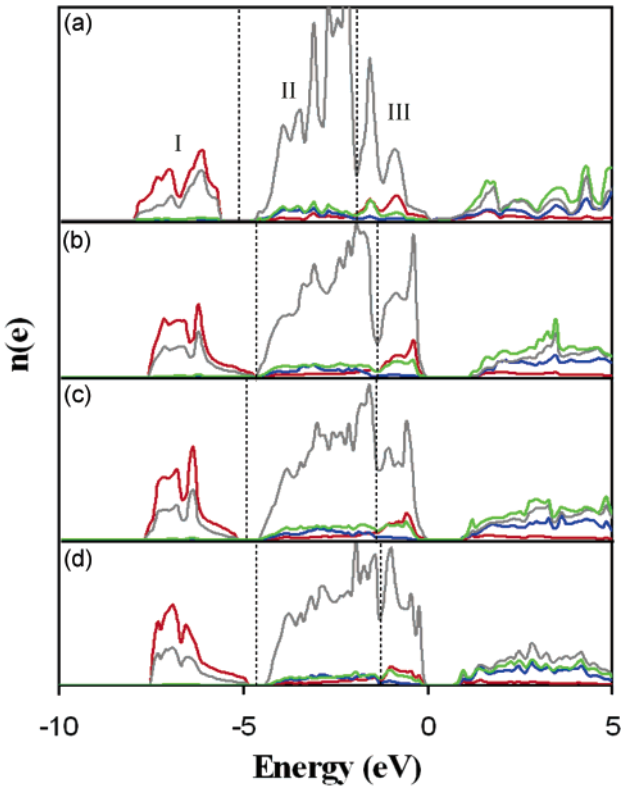

Figure 6. Partial electron density of states for (a) SnO, (b) SnS, (c) SnSe, and (d) SnTe in the herzenbergite structure, relative to the highest occupied state. The red lines correspond to Sn(5s) states, blue to Sn-($5p_x + p_y$), green to Sn($5p_z$), and gray to X(p) states. The regions of the valence band are distinguished by the dashed lines.

reduced through the series with almost no Sn(5s) character present above the Fermi level for SnTe.

The PEDOS for herzenbergite (Figure 6) share a number of common features with litharge. Regions I and II of herzenbergite SnO have similar composition to that of litharge SnO. And while Sn($5p_z$) character is again present in region III, less is present in herzenbergite SnO with a composition of approximately 70% O(2p), 20% Sn(5s), and 10% Sn($5p_z$). While herzenbergite SnO has a calculated band gap of just 0.52 eV, a band gap of 1.35 eV is calculated for herzenbergite SnS, in good agreement with the experimentally determined gap for SnS which range from 1.3[30] to 1.6 eV.[31] The gap then decreases through the series with the calculated band gap of 1.1 eV for SnSe, agreeing well with the experimental values of 1.0−1.2 eV,[26] and a band gap of 0.8 eV for SnTe in the herzenbergite structure. The PEDOS undergoes similar changes through the series to those of rocksalt and litharge with a notable reduction in the presence of anion p character in region I and of Sn(5s) present in region III. The splitting between the center of the region I Sn(5s) peak and the top of region II again increases from 4.75 eV in SnO to 5.25, 5.5, and 5.75 eV in SnS, SnSe, and SnTe, respectively.

d. Partial Electron Densities and Crystal Orbital Overlap Populations. To further examine the changes in the interactions of the Sn 5s and 5p states observed through the series, we have calculated the partial electron densities which allow the electron density arising from specific regions of the EDOS to be visualized. In addition, we have also calculated the integrated crystal orbital overlap populations[32] (COOP) to investigate the underlying interactions in more detail. These can be used to quantify the bonding between two orbital centers with positive and negative values corresponding to bonding and antibonding interactions.

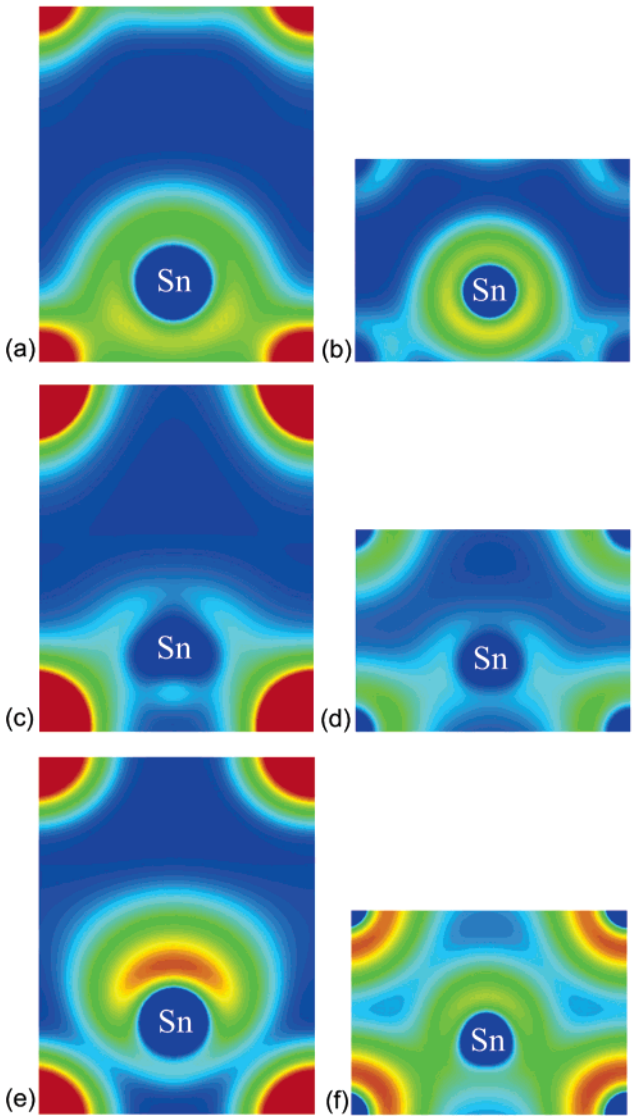

Figure 7. Partial electron density contour maps for region I of (a) litharge SnO and (b) SnTe, region II of (c) litharge SnO and (d) SnTe, and region III of (e) litharge SnO and (f) SnTe. These are taken through the (100) plane containing a Sn atom toward the center with four anions positioned at each of the corners. Contour levels are shown between 0 (blue) and 0.3 e/Å^3 (red).

The partial electron density maps for each of the regions of litharge SnO and SnTe are shown in Figure 7. For SnO, a strong bonding interaction with a large overlap of density is evident between the Sn and O atoms in region I corresponding directly with the overlap of the Sn(5s) and O(2p) states seen in the PEDOS (Figure 7a). The COOP for the Sn(5s)−X(p) interactions are included in Table 2. The large positive value of 1.4 produced for the Sn(5s)−X(p) COOP in region I of litharge SnO confirms the existence of a strong bonding interaction between Sn and O, as evident in the density maps. This is also true for the rocksalt and herzenbergite structures which have COOP values of 1.3 and 1.4, respectively. In contrast, the region I electron density map for litharge SnTe displays little overlap of density between the Sn and Te atoms (Figure 7b). With very few Te(5p) states present in this region the interaction between Sn and Te is weak, causing the Sn(5s) states to remain spherical. The COOP also reflects this change with the bonding interaction between Sn(5s) and anion p states becoming successively weakened through the series, reducing by approximately 50% from SnO to SnTe.

TABLE 2: Integrated COOPs for the Region I and Region III Sn(5s)−X(p) Interaction and the Region III Sn(5p)−X(p) Interaction for SnO, SnS, SnSe, and SnTe

		structure		
interaction	region	rocksalt	litharge	herzenbergite
Sn(5s)−O(2p)	I	1.3	1.4	1.5
Sn(5s)−S(3p)	I	0.9	1.0	1.1
Sn(5s)−Se(4p)	I	0.8	0.8	0.9
Sn(5s)−Te(5p)	I	0.7	0.7	0.8
Sn(5s)−O(2p)	III	−1.0	−0.9	−1.1
Sn(5s)−S(3p)	III	−0.7	−0.6	−0.8
Sn(5s)−Se(4p)	III	−0.6	−0.5	−0.7
Sn(5s)−Te(5p)	III	−0.5	−0.4	−0.6
Sn(5p)−O(2p)	III	0.1	0.6	0.5
Sn(5p)−S(3p)	III	0.1	0.4	0.4
Sn(5p)−Se(4p)	III	0.1	0.4	0.3
Sn(5p)−Te(5p)	III	0.1	0.2	0.2

The electron density maps arising from region II for both litharge SnO (Figure 7c) and SnTe (Figure 7d) are mainly O(2p) in nature as expected from the PEDOS and make no contribution to the asymmetric electronic distribution of Sn. The region III electron density map of litharge SnO displays an enhanced electron density pointing away from the Sn atom (Figure 7e). This is clearly the source of asymmetry in the Sn electron distribution. The absence of electron density between the Sn and O atoms would suggest an antibonding Sn(5s)−O(2p) interaction in this region. The negative COOP of −0.9 for the interaction of Sn(5s) and O(2p) in region III confirms that these are the filled antibonding states, resulting from the bonding interaction observed in region I. This interaction results in Sn(5s) states present higher in energy than expected, just below the Fermi level. Similar values are again seen for the rocksalt and herzenbergite structures showing the antibonding interaction is also present. The antibonding Sn(5s)−O(2p) states could not produce the observed asymmetric electron density on the Sn atom as together with the bonding interaction they would be expected to restore spherical symmetry.

An additional interaction is present for both litharge and herzenbergite SnO. The COOP analysis shows a strong bonding interaction between Sn(5p) and the antibonding states in region III. The asymmetric electron density is produced through constructive interference of Sn(5p) with the antibonding Sn(5s)−O(2p) states, and stabilization of the distorted phases is achieved as a result of the Sn(5p) shifting density away from the anion. This bonding interaction explains the enhanced stability of the distorted crystal structures as the coupling cannot occur in the rocksalt structure due to the symmetry of the interaction. It also explains the presence of Sn(5s) states above the Fermi level in litharge and herzenbergite SnO (produced through the antibonding combination of this interaction).

The density map for region III of SnTe displays only very faint asymmetry in the electron density around Sn (Figure 7f). Density is now present in the region between Sn and Te in line with a weaker antibonding combination. Similar to the bonding case in region I, the region III COOP for the antibonding Sn(5s)−X(p) interaction is reduced significantly from SnO to SnTe. Very few antibonding Sn(5s) states are present at the top of the valence band in SnTe. As a result, the coupling of Sn(5p) with the antibonding states is reduced to approximately 70%, 60%, and 50% their initial values in SnO for SnS, SnSe, and SnTe, respectively. The anion dependence of the "lone pair" formation of Sn(II) is clearly evident.

4. Discussion

The electron density maps show the presence of a strong directed asymmetric electron density on the Sn atoms in SnO for the structures with acentric oxygen coordination. In litharge and herzenbergite SnO, the asymmetric electron density is produced through constructive interference of Sn(5p) with the antibonding Sn(5s)−O(2p) states. Enhanced stabilization of the distorted phases is achieved as a result of the Sn(5p) shifting density away from the anion. This can be seen in the PEDOS of the asymmetric SnO structures where the near Fermi level states appear shifted to lower energies relative to the undistorted rocksalt phase where the interaction of Sn(5p) with the antibonding states is prohibited due to the symmetry of the interaction.[11] This explains the mixing of Sn(5s), Sn(5p), and O(2p) in region III at the top of the EDOS and confirms that the anion plays a role in producing the Sn lone pair.

The asymmetric electron density on Sn is seen to become less pronounced from SnO to SnTe, with the Sn electron distribution becoming more spherical through the series. From SnO to SnTe, there is a clear reduction of anion p states in region I and Sn(5s) states in region III, and these changes can be understood with the transition from O(2p) to Te(5p), with the Sn(5s) and X(p) states moving further apart, thus reducing the strength of their interaction. This results in progressively less antibonding, region III states being produced for SnS, SnSe, and SnTe with approximately 60% less Sn(5s) character present in region III of SnTe than SnO. It is only possible for Sn(5s) and Sn(5p) to couple through the mediation of the anion; therefore, as interactions with the anion are weakened, the extent of the Sn(5s)/Sn(5p) coupling is reduced, leading to weaker asymmetric electron densities in the distorted structures.

The thermodynamically stable phase of SnO is the four-coordinate, distorted litharge structure, where the Sn lone pair is considered responsible for directing the Sn−O layers. Interaction between Sn(5s) and O(2p) produces antibonding states that allow strong coupling of Sn(5p). This results in a strong, stereochemically active asymmetric density for litharge SnO. The electron density maps show that the anions with higher valence p states produce successively weaker asymmetric electron densities. These weaker lone pairs cannot support the distorted litharge structure. The equilibrium *c* lattice vector of the optimized litharge structures decreases through the series, reducing the interlayer distance. The litharge structure can be thought of as the CsCl structure with a $\sqrt{2} \times \sqrt{2}$ expansion and the *c* vector elongated to create a layered structure. The reduction seen in the *c* vector is effectively an attempt to relax back toward the undistorted CsCl structure.

The three-coordinate, herzenbergite structure is the thermodynamically stable phase of SnS and SnSe. Here a more complex layered system exists where the anions and cations are stacked along the longest axis (*a* axis). Each Sn is strongly bonded to three anions in its own layer with three weakly bound neighbors also present and can be seen as a severe distortion of the rocksalt structure. The directed asymmetric density on Sn is again considered to play an important role in layer separation. For herzenbergite SnO, the calculated *a* vector is lengthened relative to the SnS and SnSe structures. The strong anion−cation interactions again result in a strong, sterically active asymmetric density (Figure 3a), similar to that seen for litharge SnO. SnO does not adopt the herzenbergite crystal structure experimentally, and our calculations show that the structure does not adapt well to the strong asymmetry on Sn in SnO. The stacked layers are elongated along the *a* direction, producing a less stable herzenbergite structure for SnO. Considering that the anions are smaller for SnO this elongation is likely to be due to the stronger Sn lone pair. For SnS and SnSe weaker asymmetry in the Sn electron density is produced, which results in them

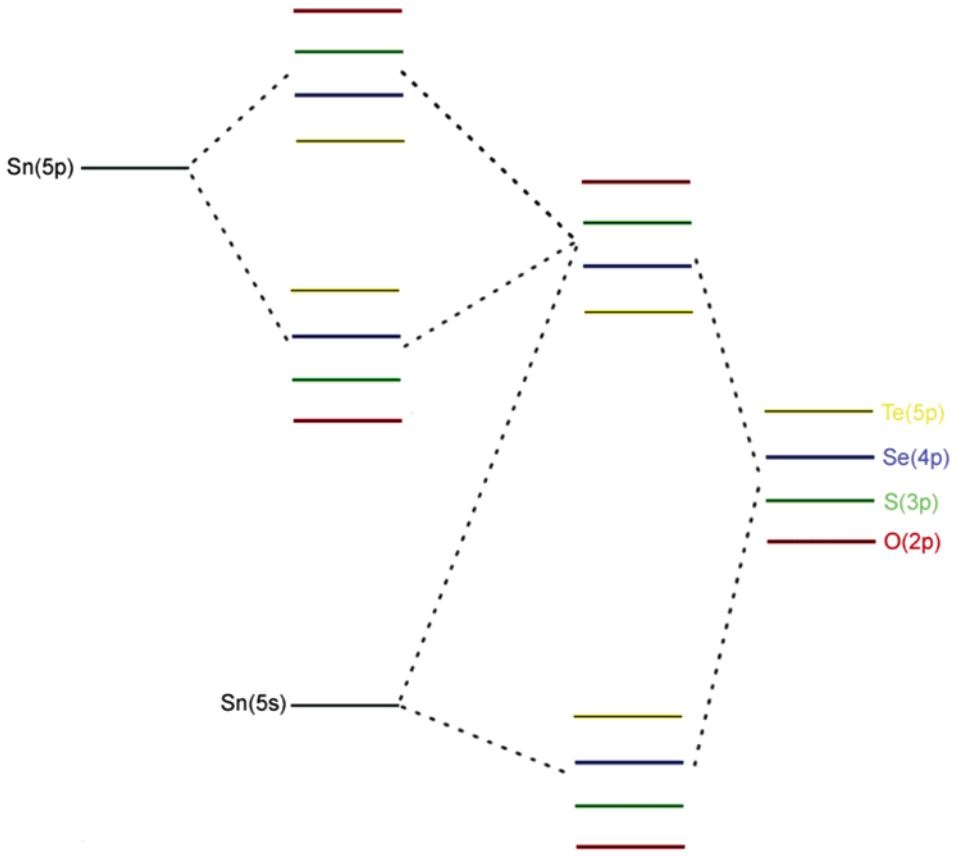

Figure 8. Schematic energy level diagram illustrating the interaction of Sn(5s) with the anion p states and the subsequent interaction of Sn(5p).

adopting the herzenbergite crystal structure. However, the coupling of Sn(5p) is restricted compared to SnO due to fewer antibonding Sn(5s) states being created. The enhanced stability of the distorted structure over undistorted rocksalt is gradually lost. While herzenbergite SnS is stable relative to the undistorted rocksalt structure, for SnSe this difference is further reduced with the rocksalt structure being energetically accessible.

For SnTe the anion−cation interactions are weaker still. The interaction of Sn(5s) and O(2p) result in almost 50% less antibonding Sn(5s) states than SnO. This makes the formation of a lone pair to stabilize either the litharge or herzenbergite structures impossible. The coupling of Sn(5p) is too weak to stabilize either distorted structure relative to a symmetric structure of higher coordination. This explains why rocksalt is adopted as the thermodynamically stable phase of SnTe.

The dependence of the directed asymmetric density on the anion can be explained schematically with the aid of an energy level diagram (Figure 8). A DFT calculation on a single Sn atom shows a splitting of 6.35 eV between the Sn(5s) and Sn(5p) states. This large separation will restrict on-site mixing of the Sn s and p orbitals. Our calculations show that the anion p states are higher in energy than the Sn(5s) states but lie in the range between Sn 5s and 5p. The interaction of Sn(5s) with the anion p states results in filled bonding and antibonding combinations. As the Sn(5s) states are lower in energy than the anion p states, the bonding combination is composed of mainly Sn(5s) character while the antibonding combination contains mainly anion p states. However, some high-energy Sn(5s) states are produced. The interaction of Sn(5s) with X(p) thus facilitates the coupling of Sn(5s) and Sn(5p), which can interact producing filled bonding and unfilled antibonding combinations. The mixing of Sn(5p) with the antibonding Sn(5s) states results in the directed asymmetric density on Sn and the stabilization of the antibonding Sn(5s) and anion p combination.

The changes observed through the series arise as the anion p states increase in energy. As shown in Figure 8, the energy of the anion p orbitals increases progressively from O to Te. The separation of Sn(5s) and the anion p states is increased, thereby reducing their interaction and resulting in less anion p character in the bonding combination and less Sn(5s) character in the antibonding combination. The largest bonding and antibonding interactions occur for oxygen while for tellurium the weakest shift is present. The strength of Sn(5s)−O(2p) interaction results in an antibonding combination with a substantial amount of Sn(5s) in comparison to interaction the other anions. This results in the strongest coupling of Sn(5p) with the antibonding states, stabilizing the antibonding Sn(5s)−O(2p) states significantly. As this interaction is reduced for each subsequent anion in the series, a less active "lone pair" is produced in each case and the enhanced stability of the distorted phases is reduced, explaining why the symmetric rocksalt structure becomes more favorable through the series and is the thermodynamically stable phase of SnTe.

5. Conclusions

The electronic structures of SnO, SnS, SnSe, and SnTe have been calculated and examined using density functional theory in the litharge, herzenbergite, and rocksalt crystal structures. In each case the most stable phase corresponds to the experimentally determined thermodynamically stable phase with good reproduction of the experimental structures. Asymmetry was found in the Sn electron distribution around the Sn atoms (the Sn lone pair) in litharge and herzenbergite SnO which became less pronounced for SnS and SnSe and with the electron distribution of Sn in SnTe almost symmetric. Examination of PEDOS, electron density maps, and COOP showed the formation of the asymmetric electron distribution exhibits strong anion

dependence through the series and confirmed that these changes arise due to changes in anion−cation interactions. This "lone pair" on Sn is not the result of hybridization of the Sn(5s) and Sn(5p) orbitals alone but is produced through the coupling of Sn(5p) with antibonding Sn(5s)−X(p) states. This coupling can only take place when there is an appropriate anion that can generate a significant amount of Sn(5s) states close to the Fermi level, as the energy difference between Sn 5s and 5p prevents them from coupling directly. While oxygen has the required energy levels for a strong interaction with Sn(5s), the higher energy valence p states of S, Se, and Te result in weaker interactions, explaining the gradual decrease in asymmetry observed in the electron density maps of the distorted structures.

The degree of asymmetry in the Sn(II) electron distribution is connected with the stability of the distorted structures. SnO, SnS, and SnSe form layered structures, driven by the stereochemical activity of the Sn(II) lone pair. The litharge phase is only energetically favorable for SnO as the strong anion−cation interactions produce a high degree of asymmetry in the electron distribution of Sn which can direct the layered structure. Any decrease in activity results in a collapse of the interlayer distance, forcing a return toward the undistorted CsCl structure and thus losing the enhanced stability of the Sn(5p) interaction and making this phase less favorable for SnS, SnSe, and SnTe. This explains why SnO is the only Sn(II) compound known to exist in this phase. SnS and SnSe adjust to their weaker Sn asymmetry by adopting the layered, herzenbergite structure as their thermodynamically stable phase which retains the rocksalt-like structure while accommodating the asymmetry of the lone pairs. This structure adapts well to the weaker SnS and SnSe asymmetry through a more closely packed layered system which has shorter Sn−Sn interatomic distances. SnO does not adopt the herzenbergite crystal structure as its lone pair is too strong to accommodate within the closer packed structure. No significant asymmetry is found in litharge or herzenbergite structured SnTe, as too few antibonding states are produced to stabilize either distorted structure relative to a symmetric structure of higher coordination. This explains why SnTe adopts the rocksalt structure as its thermodynamically stable phase.

Our calculations clearly show that the anion plays a more important role in the formation of lone pairs in Sn(II) compounds than previously thought, which has clear implications for the development of new materials. The traditional view of the Sn(II) lone pair as a chemically inactive, but sterically active, feature is shown to be incorrect with the formation of the asymmetric Sn electron density and the stability of the distorted structures requiring electronic interaction with the anion. This is the cause of the variations in crystal structure observed for different anions, explaining the unusual crystallographic behavior exhibited by Sn(II) monochalcogenides and why distorted structures are not always formed for Sn(II) compounds.

Acknowledgment. We acknowledge the HEA for a PRTLI (Cycle III) grant and TCD for a Trinity College Postgraduate Studentship. We also thank Dr. Peter Oliver at Rutherford Appleton Laboratory for access to and assistance with Mott2 and the EPSRC Grant GR/S84415/01.

References and Notes

(1) An, C.; Tang, K.; Shen, X.; Jin, Y.; Lui, Q.; Qian, Y. *J. Cryst. Growth* **2003**, *252*, 581.
(2) Timofeev, Y. A.; Vinogradov, B. V.; Begoulev, V. B. *Phys. Solid State* **1997**, *39*, 207.
(3) Odani, A.; et al. *J. Power Sources* **2003**, *119*, 517.
(4) Takeuchi, K.; et al. *Sol. Energy Mater. Sol. Cells* **2003**, *75*, 427.
(5) Orgel, L. E. *J. Chem. Soc.* **1959**, 3815.
(6) Lefebvre, I.; Lannoo, M.; Allan, G.; Ibanaz, A.; Fourcade, J.; Jumas, J. C.; Beaurepaire, E. *Phys. Rev. Lett.* **1987**, *59*, 2471.
(7) Lefebvre, I.; Lannoo, M.; Olivier-Fourcade, J.; Jumas, J. C. *Phys. Rev. B* **1991**, *44*, 1004.
(8) Pannetier, J.; Denes, G. *Acta Crystallogr., Sect. B* **1980**, *36*, 2736.
(9) Littlewood, P. B. *J. Phys. C: Solid State Phys.* **1980**, *13*, 4855.
(10) Mariano, A. N.; Chopra, K. L. *Appl. Phys. Lett.* **1967**, *10*, 282.
(11) Lefebvre, I.; Szymanski, M. A.; Olivier-Fourcade, J.; Jumas, J. C. *Phys. Rev. B* **1998**, *56*, 1896.
(12) Watson, G. W. *J. Chem. Phys.* **2001**, *114*, 758.
(13) Bernasconi, L.; Wilson, M.; Madden, P. A. *Comput. Mater. Sci.* **2001**, 22.
(14) Watson, G. W.; Parker, S. C. *J. Phys. Chem. B* **1999**, *103*, 1258.
(15) Walsh, A.; Watson, G. W. *J. Solid State Chem.* **2005**, *178*, 1422.
(16) Raulot, J. M.; Baldinozzi, G.; Seshadri, R.; Cortona, P. *Solid State Sci.* **2002**, *4*, 467.
(17) Waghmare, U. V.; Spaldin, N. A.; Kandpal, H. C.; Seshadri, R. *Phys. Rev. B* **2003**, *67*, 125111.
(18) Walsh, A.; Watson, G. W. *Phys. Rev. B* **2004**, *70*, 2535114.
(19) Kresse, G.; Hafner, J. *Phys. Rev. B* **1994**, *49*, 14251.
(20) Kresse, G.; Furthmuller, J. *Comput. Mater. Sci.* **1996**, *6*, 15.
(21) Kresse, G.; Furthmuller, J. *Phys. Rev. B* **1996**, *54*, 11169.
(22) Perdew, J. P.; Chevary, J. A.; Vorto, S. H.; Jackson, K. A.; Pedersen, M. R.; Singh, D. J.; Frolhais, C. *Phys. Rev. B* **1992**, *46*, 6671.
(23) Kohn, W.; Sham, L. J. *J. Phys. B* **1965**, *136*, 864.
(24) Blöchl, P. E. *Phys. Rev. B* **1994**, *50*, 17953.
(25) Monkhurst, H. J.; Pack, J. D. *Phys. Rev. B* **1990**, *41*, 7892.
(26) Murnaghan, F. D. *Proc. Natl. Acad. Sci. U.S.A.* **1944**, *30*, 244.
(27) Kresse, G. VASP Manual, Section 9.6, http://cms.mpi.univie.ac.at/vasp/guide/node161.html.
(28) Pearson, W. B. *Handbook of Lattice Spacing and Structure of Metals and Alloys*; Pergamon: London, 1976; Vol. 3.
(29) Guerts, J.; Rau, S.; Ritcher, W.; Schmitte, F. J. *Thin Solid Films* **1984**, *121*, 217.
(30) Parenteau, M.; Carlone, C. *Phys. Rev. B* **1990**, *41*, 5227.
(31) Valiukonis, G.; Guseinova, D. A.; Krivaite, G.; Sileika, A. *Phys. Status Solidi B* **1986**, *135*, 299.
(32) Hoffmann, R. *Solids and Surfaces*; Wiley-VCH: New York, 1988; p 42.